ISSN: 0067-2904

3D MHD Radiation Flow of Unsteady Casson Fluid with Viscous Dissipation Effect

Somireddy Sreenivasa Reddy[1], K. Govardhan[2], G. Narender [3]*, Santoshi Misra[4]
[1]*Department of Humanities and Science (Mathematics), Viganana Bharathi Institute of Technology, Hyderabad, Telangana State, India*
[2]*Department of Mathematics, GITAM University, Hyderabad, Telangana State, India*
[3]*Department of Humanities and Sciences (Mathematics), CVR College of Engineering, Hyderabad, Telangana State, India*
[4]*Departmet of Mathematics, St. Ann's College for Women, Hyderabad, Telangana State, India*

Received: 24/4/2022 Accepted: 17/9/2022 Published: 30/8/2023

Abstract
A numerical evaluation of the crucial physical properties of a 3D unsteady MHD flow along a stretching sheet for a Casson fluid in the presence of radiation and viscous dissipation has been carried out. Meanwhile, by applying similarity transformations, the nonlinear partial differential equations (PDEs) are transformed into a system of ordinary differential equations (ODEs). Furthermore, in the numerical solution of nonlinear ODEs, the shooting method along with Adams Moulton method of order four has been used. The obtained numerical results are computed with the help of FORTRAN. The tables and graphs describe the numerical results for different physical parameters which affect the velocity and temperature profiles.

Keywords: Magnetohydrodynamic, thermal radiation, Casson fluid, viscous dissipation, Adams-Moulton method.

1. Introduction

During the past few decades, the boundary layer problems related to a stretching surface have attracted extensive attention of researchers, because the number of applications related to this area is found in engineering and industrial manufacturing processes. Actually, the boundary layer has a meaningful concept in physics and fluid mechanics, which is introduced as the layer of the fluid in the region of a bounded area where the effects of viscosity are powerful. Moreover, it is also a region in the flow field in which the fluid deforms with a relative velocity. Each primary fluid has some basic important properties which play an essential role in its dynamics. The stretching and cooling rates both are significant in the manufacturing process for the effective results of the final product. A speedy change in stretching damages the final product because of sudden solidification, so it is essential to maintain the stretching rate. The 2D flow of an incompressible liquid within the boundary layer along the stretching surface was first presented by Crane [1]. Various researchers have studied the interesting fluid flow along a stretching sheet [2-5].

Magnetohydrodynamics (MHD) is a combination of three words, magneto means magnetic field, hydro means water and dynamics means movements. Meanwhile hydromagnetic flow is

*Email: gnriimc@gmail.com

the analysis of the magnetic properties of an electrically conducting fluid. Plasmas, liquid metals, saltwater, and electrolytes are considered magneto fluids. MHD flow has a wide range of applications in engineering devices such as the design of heat exchanges, blood pumping machines and the MHD electric power generators. The main role of a magnetic parameter in the flow field is to produce a resistive force which maintains the flow and detains the boundary layer separation. A number of researchers investigated the flow models which contain the hydromagnetic effects. On top of that, Pavlov [6] examined the MHD flow of viscous fluids along a stretching sheet. Alfven [7] established the existence of electromagnetic-hydro-dynamic waves. Sarpakaya [8] studied the flow of specific types of fluids in the magnetic field.

The time-dependent flows are considered as unsteady flow. Wang [9] investigated the time dependent flow problems. Furthermore, various researchers considered the impacts of induced magnetic field on the time dependent MHD flow within the boundary layer region [10-12]. Ishak et al. [13] studied the heat transfer of a time dependent flow. The temperature variation between the surrounding and the ambient fluid, produce the radiation.

The complicated behavior of stress-strain can be found in a type of fluids which is called non-Newtonian fluids. Moreover, non-Newtonian fluids have earned considerable attention because a number of applications of these fluids are found in engineering and industry. The Casson fluid is one of the most important non-Newtonian fluids, which is used in metallurgy, food processing etc. Casson [14] introduced the Casson fluid model for the pigment-oil suspensions. Casson fluid exhibits the properties of yield stresses. Whenever the shear stress is greater than the yield stress, the fluid acts like a liquid. Likewise, if shear stress is less than the yield stresses the fluid acts like a solid. In the category of Casson fluids, Jelly, shampoo, toothpaste, ketchup, tomato sauce, honey, soup and juices are founded. Actually, yield stress analysis is important for all complex structured fluids. Dash et al. [15] examined the Casson fluid inside a pipe containing a porous medium Later on Eldabe et al. [16] investigated the hydromagnetic flow of a Casson fluid bounded between two cylinders in a rotating position. Later on, several researchers worked on the free convective electromagnetic flow of Casson fluid in various conditions [17-21]. Maleque [22] investigated the MHD flow of Casson liquid along with a rotating disk. Kataria and Patel [23] considered the ramped wall temperature with heat and mass transfer in the hydromagnetic flow of Casson liquid through a porous medium. The MHD Casson fluid with the effects of Hall, Dufour and thermal radiation was analyzed by Vijayaragavan and Karthikeyan [24]. G. Narender et al. [25] studied the impact of the radiation effects in the presence of heat generation/absorption and magnetic field on the magnetohydrodynamics (MHD) stagnation point flow over a radially stretching sheet using a Casson nanofluid. G. Narender et al. [26] examined the viscous dissipation and thermal radiation effects on the MHD mixed convection stagnation point flow of Maxwell nanofluid over a stretching surface. G. Narender et al. [27] explored the impacts of external magnetic field inclinations and viscous dissipation due to heat generation or absorption parameter on MHD mixed convective flow of Casson nanofluid.

The detailed review work of Parshu and Nankeolyar [28] is explained in this article and extended by considering viscous dissipation. The numerical solution of various parameters has been discussed which impact the skin friction coefficients, Nusselt number, velocity and temperature. Investigation of obtained numerical results is given through tables and graphs.

2. Mathematical Modelling

A 3D time-dependent, magnetohydrodynamic flow of an incompressible Casson fluid along a linearly stretchable surface has been examined. Meanwhile, the surface is along the plane,

which means that $y = 0$ and the fluid confined along the positive direction of $y-$ axis has been considered. Furthermore, the sheet is considered to be stretched along $x-$ axis. The time dependent magnetic field has been assumed to act along y-axis which is normal to the surface of the sheet. The physical model of flow is given below in Figure 1. Here u_w is the stretching sheet velocity along the $x-$direction, the surface temperature is T_w and the disposition temperature is T_∞. The system of equations describing the flow has been given below, which contains the PDEs of continuity equation, momentum, and energy transfer [28].

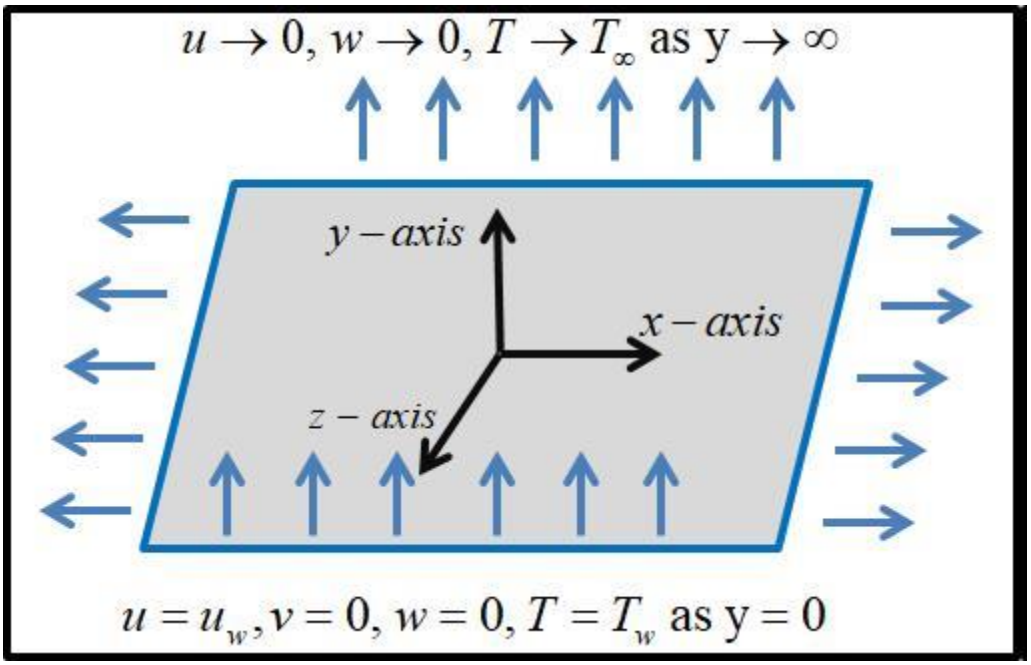

Figure 1: Schematic representation of physical model.

$$\frac{\partial u}{\partial x}+\frac{\partial v}{\partial y}+\frac{\partial w}{\partial z}=0, \tag{1}$$

$$\frac{\partial u}{\partial t}+\frac{\partial u}{\partial x}u+\frac{\partial u}{\partial y}v+\frac{\partial u}{\partial z}w=\nu\left(1+\frac{1}{\beta}\right)\left(\frac{\partial^2 u}{\partial y^2}\right)-\frac{\sigma B^2(t)}{\rho\left(1+m^2\right)}(u+mw), \tag{2}$$

$$\frac{\partial w}{\partial t}+\frac{\partial w}{\partial x}u+\frac{\partial w}{\partial y}v+\frac{\partial w}{\partial z}w=\nu\left(1+\frac{1}{\beta}\right)\left(\frac{\partial^2 w}{\partial y^2}\right)-\frac{\sigma B^2(t)}{\rho\left(1+m^2\right)}(mu-w), \tag{3}$$

$$\frac{\partial T}{\partial t}+\frac{\partial T}{\partial x}u+\frac{\partial T}{\partial y}v+\frac{\partial T}{\partial z}w=-\frac{\nu}{\rho}\left(1+\frac{1}{\beta}\right)\left(\frac{\partial u}{\partial y}\right)^2+\alpha_m\left(\frac{\partial^2 T}{\partial y^2}\right)-\frac{1}{\left(\rho c_p\right)}\frac{\partial q_r}{\partial y} \tag{4}$$

The associated boundary conditions can be written as:

$$\left.\begin{aligned} &y=0: u=U_w(x), v=0, w=0, T=T_w,\\ &y\to\infty: u\to\infty, w\to\infty, T\to T_\infty. \end{aligned}\right\} \tag{5}$$

The Casson liquid parameter is denoted by β, the electrical conductivity by σ, density by ρ, the kinematic viscosity by ν, Hall current by m, the temperature by T, the thermal diffusivity by $\alpha_m = \frac{k}{\rho c_p}$. Furthermore the wall stretching velocity with time dependent by

$u_w(x,t)=\frac{ax}{1-\gamma t}$ [28] and the magnetic field with time dependent by $B(t)=B_0(1-\gamma t)^{-\frac{1}{2}}$, [28]

where a and γ are constants and B_0 the magnetic strength.

The radiative heat flux q_r [28] can be written as

$$q_r=-\frac{4\sigma^*}{3\alpha^*}\frac{\partial T^4}{\partial y}=-\frac{16\sigma^*}{3\alpha^*}T^3\frac{\partial T}{\partial y} \tag{6}$$

where the Stefan-Boltzmann constant is σ^* and the coefficient of Rosseland mean absorption is α^*. From (6), putting q_r into (4) and after a little simplification, we get

$$\frac{\partial T}{\partial t}+\frac{\partial T}{\partial x}u+\frac{\partial T}{\partial y}v+\frac{\partial T}{\partial z}w=-\frac{\nu}{\rho}\left(1+\frac{1}{\beta}\right)\left(\frac{\partial u}{\partial y}\right)^2+\frac{\partial}{\partial y}\left(\left(\alpha_m+\frac{16\sigma^*T^3}{3\alpha^*\rho c_p}\right)\frac{\partial T}{\partial y}\right). \tag{7}$$

For the conversion of the mathematical model (2)-(4) into the dimensionless form, the following similarity transformation [28] has been introduced,

$$\left.\begin{aligned} &u=\frac{ax}{1-\gamma t}f'(\eta),\ v=-\sqrt{\frac{a\nu}{1-\gamma t}}f(\eta),\ w=\frac{ax}{1-\gamma t}g(\eta),\\ &\theta(\eta)=\frac{T-T_\infty}{T_f-T_\infty},\ \eta=y\sqrt{\frac{a}{\nu(1-\gamma t)}}. \end{aligned}\right\} \tag{8}$$

The final dimensionless form of the governing model, is

$$\left(1+\frac{1}{\beta}\right)f'''+ff''-(f')^2-A\left(f'+\frac{\eta}{2}f''\right)-\frac{M}{1+m^2}(f'+mg)=0, \tag{9}$$

$$\left(1+\frac{1}{\beta}\right)g''-gf'+fg'-A\left(g+\frac{\eta}{2}g'\right)+\frac{M}{1+m^2}(mf'-g)=0, \tag{10}$$

$$\left(1+\frac{4}{3N_r}\left(1+(tr-1)\theta\right)^3\right)\theta''-\Pr A\frac{\eta}{2}\theta'+\Pr f\theta'+\Pr\left(1+\frac{1}{\beta}\right)Ec\,f''+\left(\frac{4}{3N_r}(tr-1)\left(1+(tr-1)\theta\right)^2\right)(\theta^1)^2=0, \tag{11}$$

The associated BCs (5) shown as

$$\left.\begin{aligned} &\eta=0:\ f(\eta)=0,\ f'(\eta)=1,\ g(\eta)=0,\ \theta(\eta)=1,\\ &\eta\to\infty:\ f'(\eta)\to 0,\ g(\eta)\to 0,\ \theta(\eta)\to 0. \end{aligned}\right\} \tag{12}$$

Different parameters used in (9)-(11) are defined as follow [28]:

$$\left.\begin{aligned} &A=\frac{\gamma}{a},\ M=\frac{\sigma B_0^2}{\rho a},\ N_r=\frac{k\alpha^*}{4\sigma^*T_\infty^3}\Pr=\frac{\nu}{\alpha_m},\ tr=\frac{T_w}{T_\infty},\ Ec=\frac{a^2x^2}{\alpha c_p(T_w-T_\infty)} \end{aligned}\right\} \tag{13}$$

The skin friction coefficient along $x-$ direction, $z-$ direction and the local Nusselt number are defined as [28]:

$$C_{fx}=\frac{\tau_{wx}}{\rho u_w^2},\ C_{fz}=\frac{\tau_{wz}}{\rho u_w^2},\ Nu_x=\frac{xq_w}{k(T_w-T_\infty)} \tag{14}$$

Given below are the formulae for τ_w, q_w and q_m [28].

$$\tau_{wx}=\mu\left(1+\frac{1}{\beta}\right)\left(\frac{\partial u}{\partial y}\right)_{y=0},\tau_{wz}=\mu\left(1+\frac{1}{\beta}\right)\left(\frac{\partial w}{\partial y}\right)_{y=0},q_w(x)=-k\left(\frac{\partial T}{\partial y}-\frac{q_r}{k}\right)_{z=0}. \tag{15}$$

The transformation of the above formulae into the dimensionless form has been carried out as:

$$\left.\begin{aligned} &C_{fx}\sqrt{\mathrm{Re}}_x=\left(1+\frac{1}{\beta}\right)f''(0),C_{fz}\sqrt{\mathrm{Re}}_x=\left(1+\frac{1}{\beta}\right)g'(0),\\ &\frac{Nu_x}{\sqrt{\mathrm{Re}}_x}=-\left[1+\frac{4}{3N_r}\left(1+(t-1)\theta(0)\right)^3\right]\theta'(0). \end{aligned}\right\} \tag{16}$$

where, τ_{wx} and τ_{wz} denotes the shear stress components, q_w by the heat transfer rate and $\mathrm{Re}_x=\frac{xu_w}{\nu}$ elucidates the local Reynolds number.

3. Method of Solution

For the solution of ODEs (9)-(11), the shooting method has been used. The dimensionless equations (9) and (10) are coupled in f and g. These two equations will be solved separately by the shooting method. Later on, the solution of (9) and (10) will be used in (11) as a known input. The missing initial conditions (ICs) $f''(0)$ and $g'(0)$ are denoted by r and s. For further improvement of the missing conditions, Newton's method will be used. Furthermore, the following notations have been incorporated.

$$\left.\begin{aligned} &f=h_1,f'=h_2,f''=h_3,g=h_4,g'=h_5,\\ &\frac{\partial f}{\partial r}=h_6,\frac{\partial f'}{\partial r}=h_7,\frac{\partial f''}{\partial r}=h_8,\frac{\partial g}{\partial r}=h_9,\frac{\partial g'}{\partial r}=h_{10},\\ &\frac{\partial f}{\partial s}=h_{11},\frac{\partial f'}{\partial s}=h_{12},\frac{\partial f''}{\partial s}=h_{13},\frac{\partial g}{\partial s}=h_{14},\frac{\partial g'}{\partial s}=h_{15}. \end{aligned}\right\} \tag{17}$$

The above mathematical models (9)-(10), now be listed in the form of the following first order coupled ODEs.

$$h_1' = h_2, \qquad h_1(0) = 0,$$
$$h_2' = h_3, \qquad h_2(0) = 1,$$
$$h_3' = \frac{\beta}{1+\beta}\left[A\left(h_2 + \frac{\eta}{2}h_3\right) - h_1h_3 + h_2^2 + \frac{M}{1+m^2}\left(h_2 + mh_4\right)\right], \qquad h_3(0) = r,$$
$$h_4' = h_5, \qquad h_4(0) = 0,$$
$$h_5' = \frac{\beta}{1+\beta}\left[A\left(h_4 + \frac{\eta}{2}h_5\right) + h_4h_2 - h_1h_5 - \frac{M}{1+m^2}\left(mh_2 - h_4\right)\right], \qquad h_5(0) = s,$$
$$h_6' = h_7, \qquad h_6(0) = 0,$$
$$h_7' = h_8, \qquad h_7(0) = 0,$$
$$h_8' = \frac{\beta}{1+\beta}\left[A\left(h_7 + \frac{\eta}{2}h_8\right) - h_1h_8 - h_3h_6 + 2h_2h_7 + \frac{M}{1+m^2}\left(h_7 + mh_9\right)\right], \qquad h_8(0) = 1,$$
$$h_9' = h_{10}, \qquad h_9(0) = 0,$$
$$h_{10}' = \frac{\beta}{1+\beta}\left[A\left(h_9 + \frac{\eta}{2}h_{10}\right) + h_4h_7 + h_9h_2 - h_1h_{10} - h_6h_5 - \frac{M}{1+m^2}\left(mh_7 - h_9\right)\right], \qquad h_{10}(0) = 0,$$
$$h_{11}' = h_{12}, \qquad h_{11}(0) = 0,$$
$$h_{12}' = h_{13}, \qquad h_{12}(0) = 0,$$
$$h_{13}' = \frac{\beta}{1+\beta}\left[A\left(h_{12} + \frac{\eta}{2}h_{13}\right) - h_1h_{13} - h_3h_{11} + 2h_2h_{12} + \frac{M}{1+m^2}\left(h_{12} + mh_{14}\right)\right], \qquad h_{13}(0) = 0,$$
$$h_{14}' = h_{15}, \qquad h_{14}(0) = 0,$$
$$h_{15}' = \frac{\beta}{1+\beta}\left[A\left(h_{14} + \frac{\eta}{2}h_{15}\right) + h_4h_{12} + h_{14}h_2 - h_1h_{15} - h_{11}h_5 - \frac{M}{1+m^2}\left(mh_{12} - h_{14}\right)\right], \quad h_{15}(0) = 1,$$

The above IVP will be solved numerically by the Adams-Moulton method. To get the approximate solution, the domain of the problem has been taken as $[0, \eta_\infty]$ instead of $[0, \infty)$, where η_∞ is an appropriate finite positive real number. In the above system of equations, the missing conditions r and s, must be chosen in such a way that

$$h_2(\eta_\infty, r, s)_s = 0, \qquad h_4(\eta_\infty, r, s)_s = 0 \tag{18}$$

For the improvement of the missing condition, Newton's method has been implemented which is conducted by the following iterative scheme:

$$\begin{bmatrix} r^{(k+1)} \\ s^{(k+1)} \end{bmatrix} = \begin{bmatrix} r^{(k)} \\ s^{(k)} \end{bmatrix} - \left[\begin{bmatrix} h_7 & h_9 \\ h_{11} & h_{14} \end{bmatrix}^{-1} \begin{bmatrix} h_2 \\ h_4 \end{bmatrix} \right]_{\left(r^{(k)}, s^{(k)}, \eta_\infty\right)} \tag{19}$$

The following steps are involved for the accomplishment of the shooting method.

(i) Choice of the guesses $r = r^{(0)}$ and $s = s^{(0)}$.

(ii) Choice of a positive small number ε.

If $\max\left\{\left|y_2(\eta_\infty) - 0\right|, \left|y_4(\eta_\infty) - 0\right|\right\} < \varepsilon$, the process is terminated, otherwise go to (iii).

(iii) Compute $r^{(k+1)}$ and $s^{(k+1)}$, $k = 0,1,2,3,.....,$ by using (19).

(iv) Repeat (i) and (ii).

In a similar manner, the ODE (11) along with the associated BCs can be solved by considering f as a known function.

4. Representation of Graphs and Tables

The physical impacts of significant parameters on the skin friction coefficients and Nusselt number have been explained through graphs and tables. Prashu and Nankeolyar [28] used the spectral Quasilinearization method (SQLM) for the numerical solution of the discussed model. In the present survey, the shooting method along with Adams-Moulton Method has been opted for reproducing the solution of [28]. The results discussed in Table 4.1, reflect the impacts of significant parameters on the skin friction coefficients $-C_{fx}\,\mathrm{Re}^{\frac{1}{2}}$ and $-C_{fz}\,\mathrm{Re}^{\frac{1}{2}}$.

The results are compared with those of Prashu and Nankeolyar [28] showing an excellent agreement. For the rising values of the M, skin friction coefficient increases in both x and z direction. The skin friction coefficient decreases in both x and z direction due to ascending values of the β Casson parameter. Furthermore, the accelerating values of m Hall current decrease the $-C_{fx}\,\mathrm{Re}^{\frac{1}{2}}$ and increase $-C_{fz}\,\mathrm{Re}^{\frac{1}{2}}$. Likewise, by increasing the values of unsteadiness A, there is a marginal increment in the skin friction coefficient along the x axis and a decrement along the z axis.

Table 4.1: Results of the $-C_{fx}\,\mathrm{Re}^{\frac{1}{2}}$ and $-C_{fz}\,\mathrm{Re}^{\frac{1}{2}}$ for various parameters.

M	m	A	β	$-C_{fx}\,\mathrm{Re}^{\frac{1}{2}}$		$-C_{fz}\,\mathrm{Re}^{\frac{1}{2}}$	
				[28]	**Present**	**[28]**	**Present**
6	0.1	0.1	0.3	5.51874456	5.518748000	0.23905696	0.239053200
2				3.63997437	3.640760000	0.12517671	0.124864700
8				6.24973648	6.249738000	0.27988605	0.279885500
	0.5			5.15310039	5.153086000	1.03810463	1.038099000
	1.0			4.47154368	4.471480000	1.50968576	1.509767000
		0.13		5.52749427	5.527499000	0.23866458	0.238661000
		0.15		5.53332180	5.533327000	0.23840377	0.238400300
			0.5	4.59187303	4.591874000	0.19890741	0.198907200
			0.6	4.32925941	4.329258000	0.18753170	0.187531600

In Table 4.2, the effects of the significant parameters on Nusselt number $Nu_x\,\mathrm{Re}^{-\frac{1}{2}}$ have been discussed. The growing pattern is found in the $Nu_x\,\mathrm{Re}^{-\frac{1}{2}}$ due to the accelerating values of m, Prandtl number Pr and temperature ratio tr, while the magnetic parameter M, unsteadiness parameter A and Casson parameter β cause a decrement in the Nusselt number.

Table 4.2: Results of the $Nu_x \operatorname{Re}^{-\frac{1}{2}}$ for various parameters.

M	m	A	Nr	tr	β	Pr	$Nu_x \operatorname{Re}^{-\frac{1}{2}}$	
							[28]	Present
6	0.1	0.1	2	1	0.3	10	2.68073953	2.680741
2							2.85395341	2.853843
8							2.61197510	2.611977
	0.5						2.70970177	2.709705
	1.0						2.76677553	2.766787
		0.13					2.64303470	2.643035
		0.15					2.61732067	2.617321
			4				2.44614512	2.446145
			6				2.35862695	2.358628
				2			3.86324873	3.863249
				3			5.08255834	5.082558
					0.5		2.57918784	2.575941
					0.6		2.54083532	2.537679
						15	3.39809230	3.398094
						20	4.00188854	4.001891

Figures 4.2 – 4.4 shows the effects of different parameters on the velocity and temperature respectively. Figure 4.2 shows the decreasing behavior of velocity along the x direction, due to rising values of the β and the M. Actually, the β reveals the properties of yield stress. Stabilization effects are also found by extending the yield stress. The impacts of applied magnetic field give rise to a resistive force in flow field called the Lorentz force. Figure 4.3 reflects that the increasing values of the Casson parameter β and the magnetic field M, the velocity profile along the z – axis increases near the boundary surface and then starts reducing away from the boundary surface. The temperature profile accelerates due to rising values of the β and M which is illustrated in Figure 4.4.

Furthermore, the effects of significant parameters, the Hall Current m and the unsteadiness A on the velocity behaviors and the temperature profile are illustrated in Figures 4.5 – 4.7 when the power of the magnetic field is strong then no one can neglect the effect of Hall current because the utilization of the magnetic field with electrically conducting fluid produces Hall current m. Figures 4.5 (a) and (b) illustrate the effects of the m and the A on the velocity profile along the x direction. By ascending values of m, the velocity profile is also increased, while increasing values of the unsteadiness A, there is a marginal decay in the velocity profile. Figures 4.6 (a) and (b) show the effects of the m and the A on the velocity profile along the z direction. The increasing values of the m, there is a significant rise in the velocity profile, while for the increasing values of the A, there is a marginal decrement in the velocity profile within boundary layer region. Figures 4.7 (a) and (b) show the impact of the m and the A on the temperature. Meanwhile the temperature is a reducing function of the Hall current m and by increasing the values of the unsteadiness A, there is a marginal enhancement in the temperature behavior. By ascending values of the Hall current m, are found to enhance the thickness of the momentum boundary layer. However, by accelerating values of the unsteadiness A, the thermal boundary layer becomes thick.

The influence of the significant parameters on the temperature behavior is shown in Figures 4.8–4.11 respectively. In Figure 4.8, the rising values of radiative parameter Nr, the temperature is reduced because the temperature distribution is inversely proportion to the Nr. In Figure 4.9 shows that the greater values of Prandtl number $\Pr$ has shrink the temperature profile. However, $\Pr$ is the ratio of the viscous diffusion to the thermal diffusion. Figure 4.10 portrays that the increasing values of temperature ratio tr, the temperature profile shows a growing behavior. Actually, tr is a ratio between temperature behavior at the surface to the temperature behavior beyond the surface. Further, Figure 4.11 is delineated to show the impact of Ec on the temperature field $\theta(\eta)$. This graph exhibits that by enhancing the estimations of Ec, the temperature field $\theta(\eta)$ is also increased.

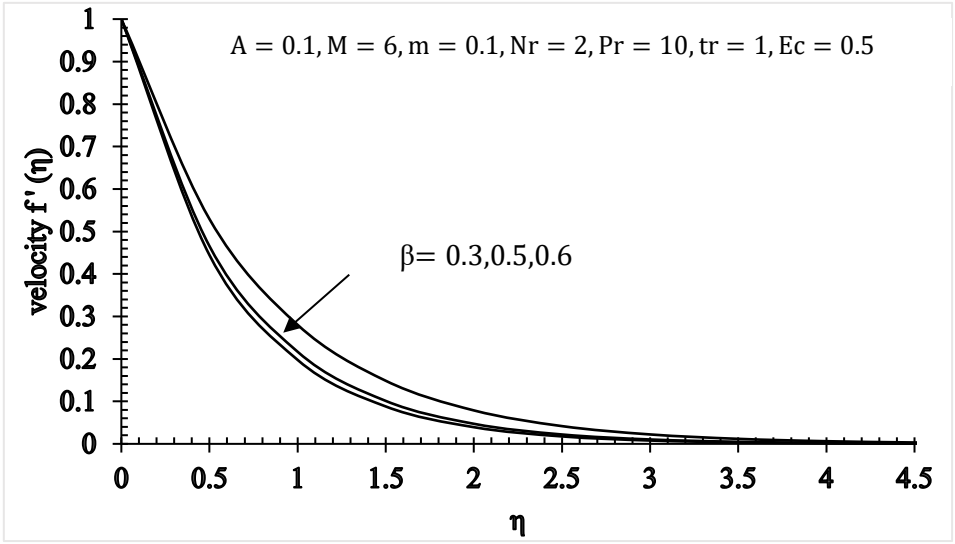

(a)

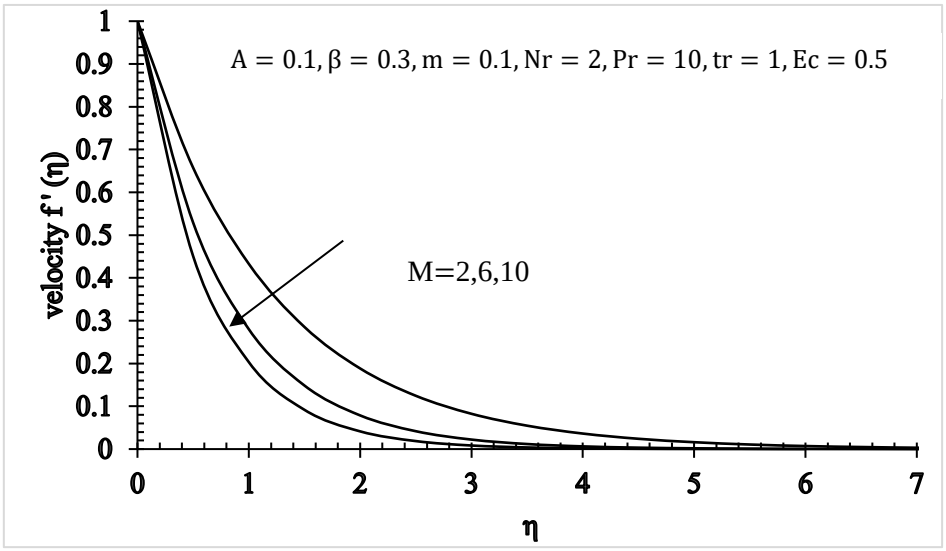

(b)

Figure 4.2: Change in $f^{''}(\eta)$ for rising values of β and M.

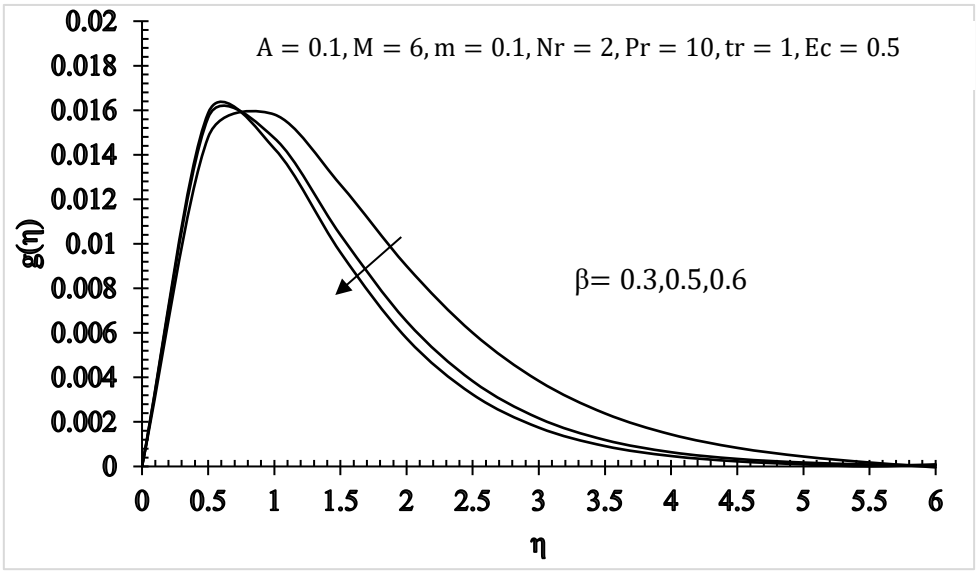

(a)

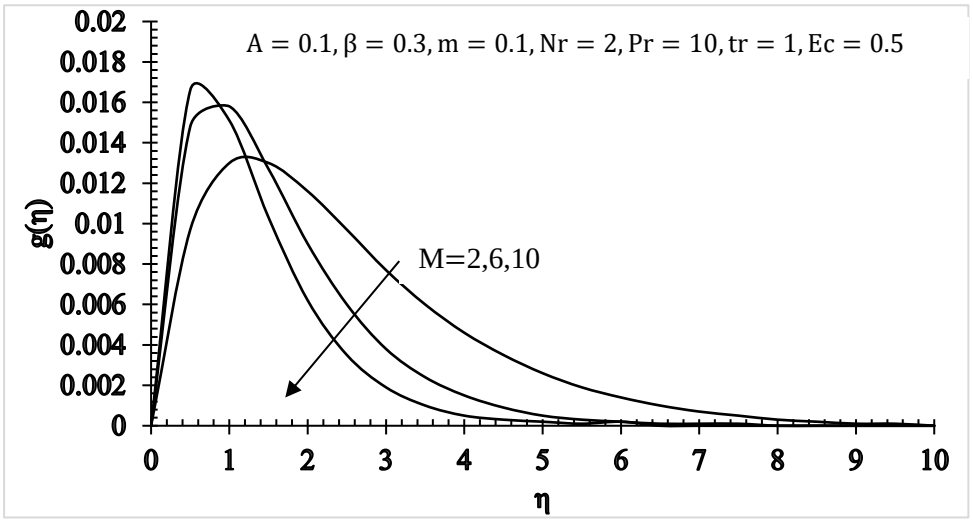

(b)

Figure 4.3: Change in $g(\eta)$ for rising values of β and M.

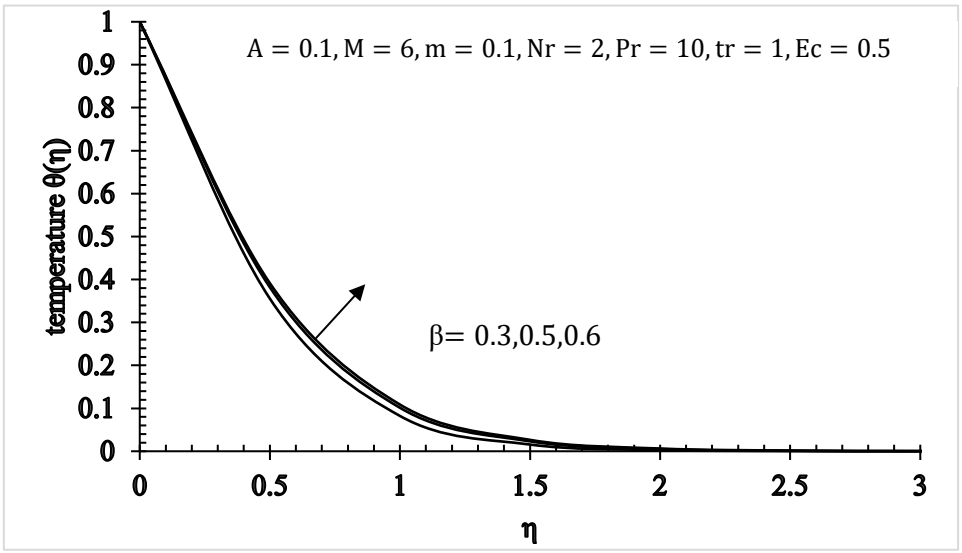

(a)

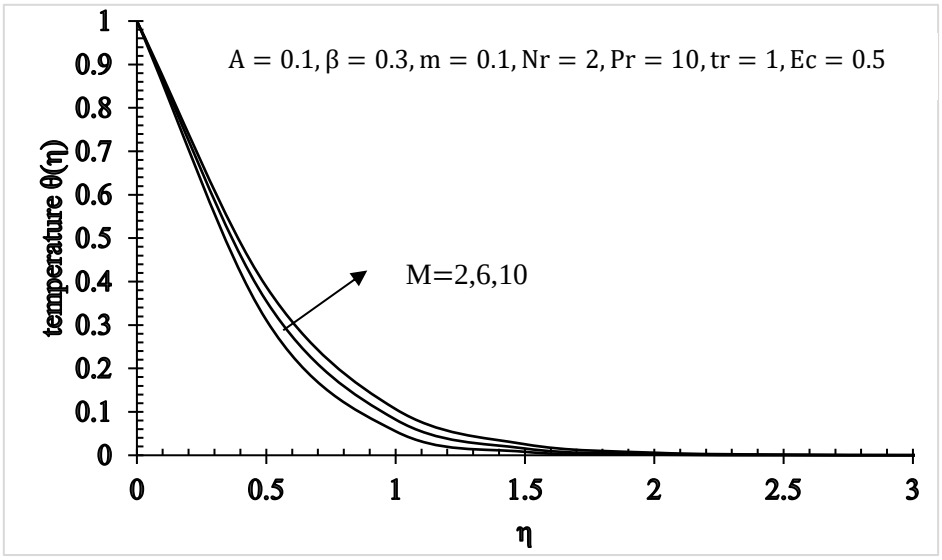

(b)

Figure 4.4: Change in $\theta(\eta)$ for rising values of β and M.

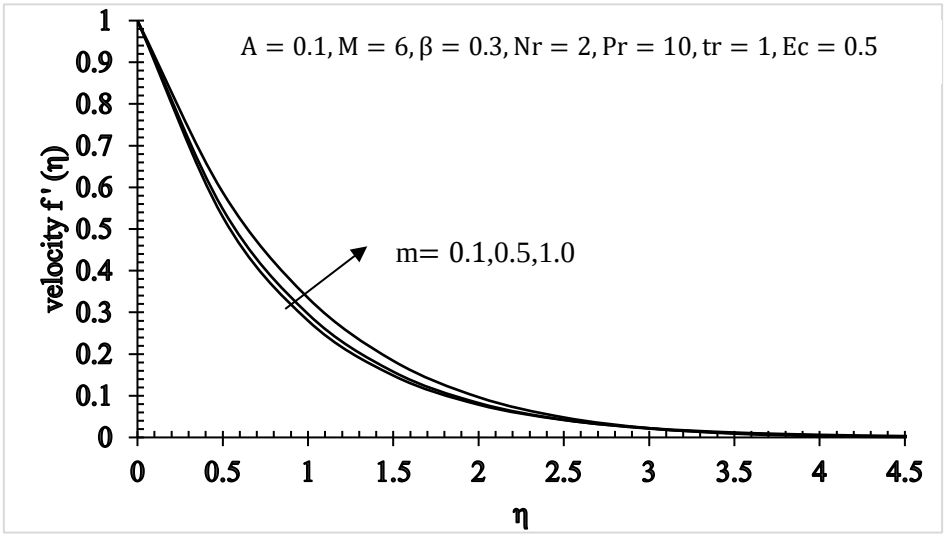

(a)

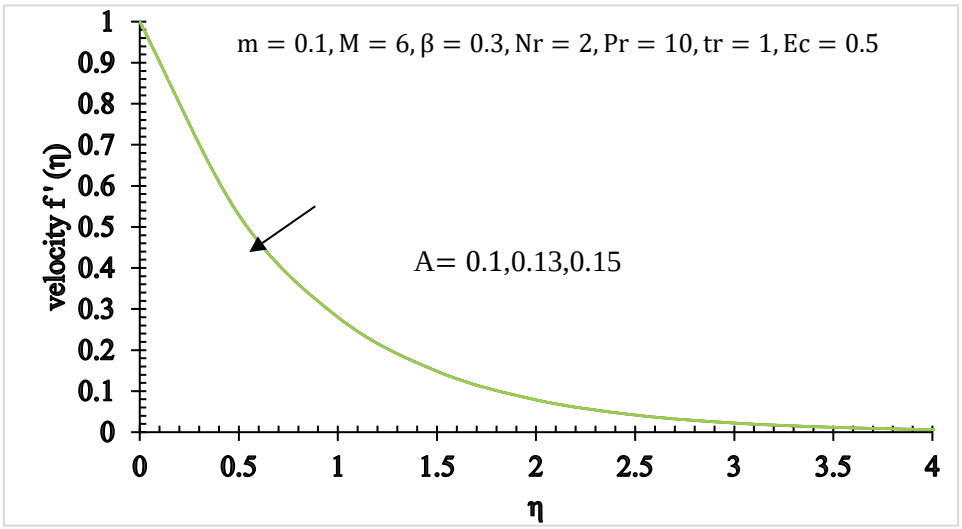

(b)

Figure 4.5: Change in $f^{''}(\eta)$ for rising values of m and A.

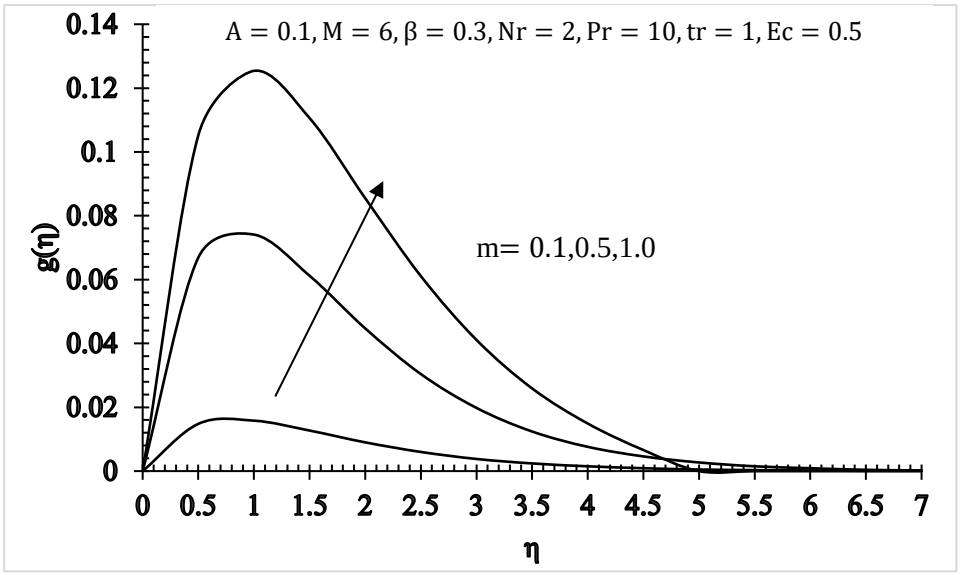

(a)

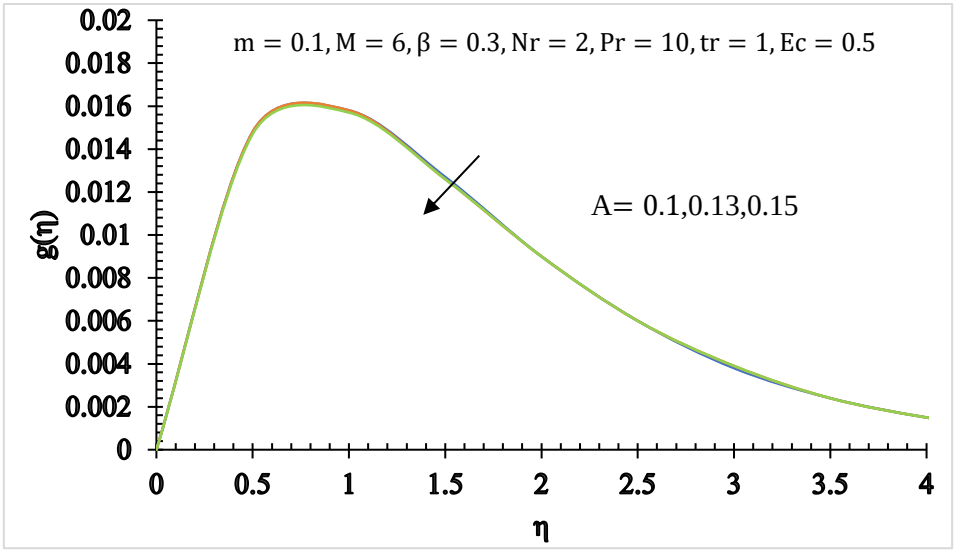

(b)

Figure 4.6: Change in $g(\eta)$ for rising values of m and A.

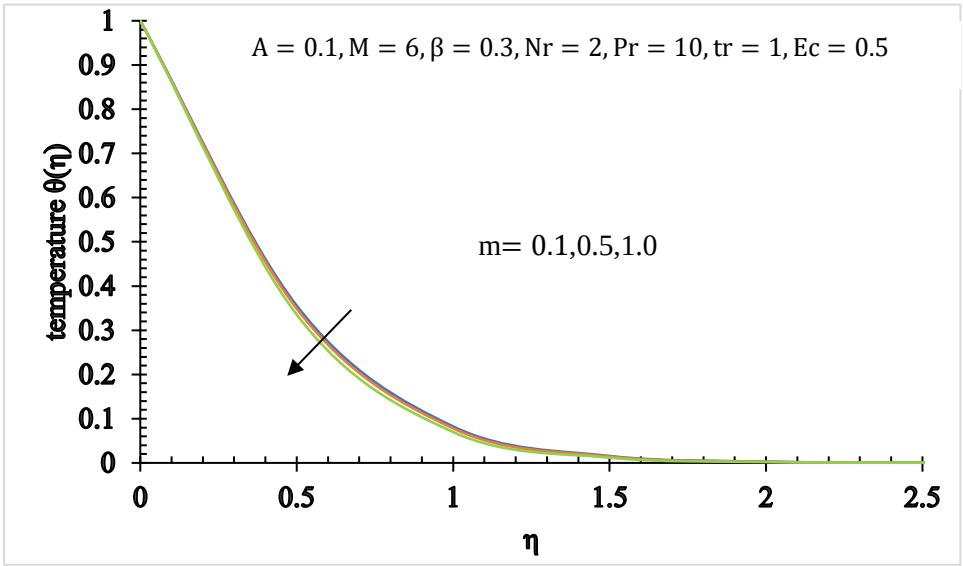

(a)

(b)

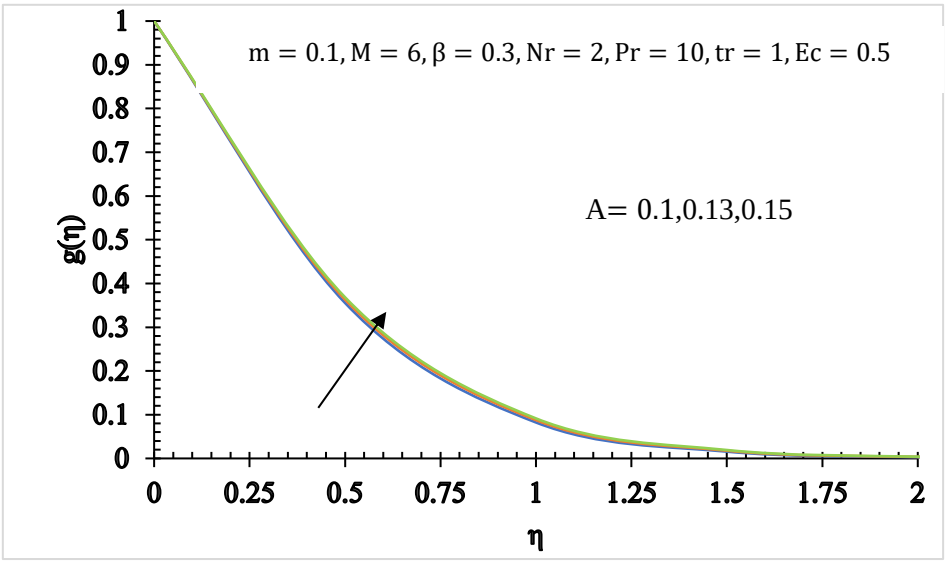

Figure 4.7: Change in $\theta(\eta)$ for rising values of m and A.

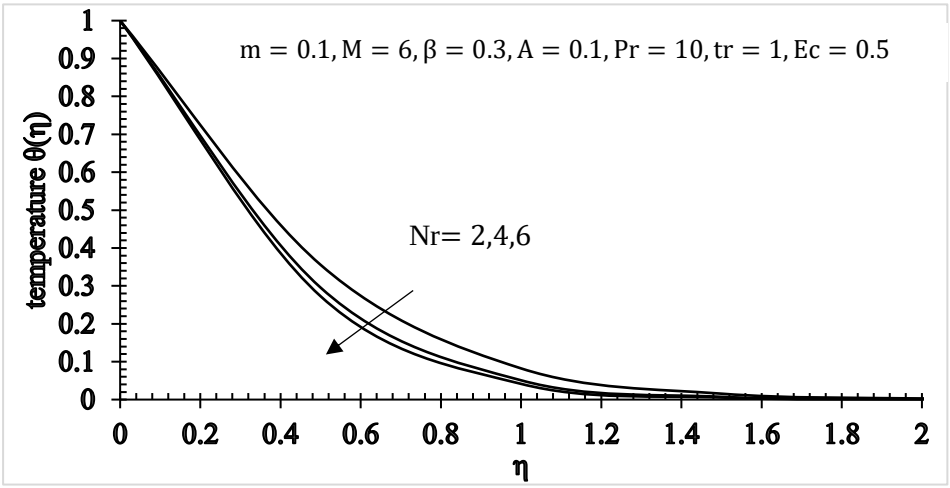

Figure 4.8: Change in $\theta(\eta)$ for ascending values of Nr.

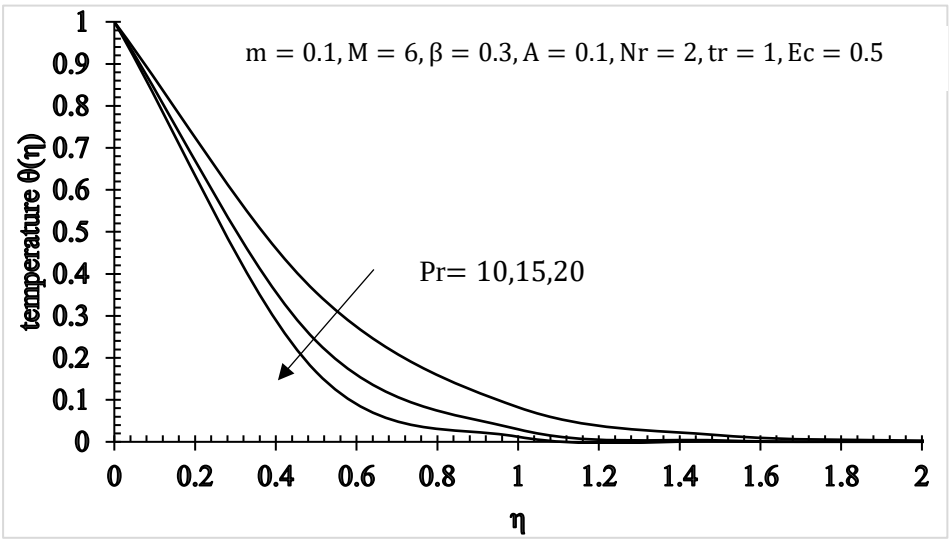

Figure 4.9: Change in $\theta(\eta)$ for ascending values of Pr.

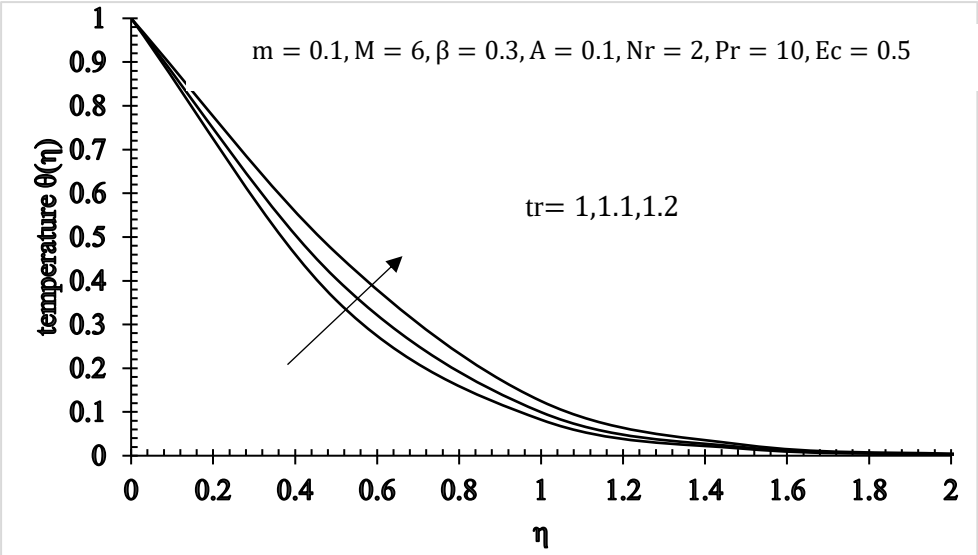

Figure 4.10: Change in $\theta(\eta)$ for ascending values of tr .

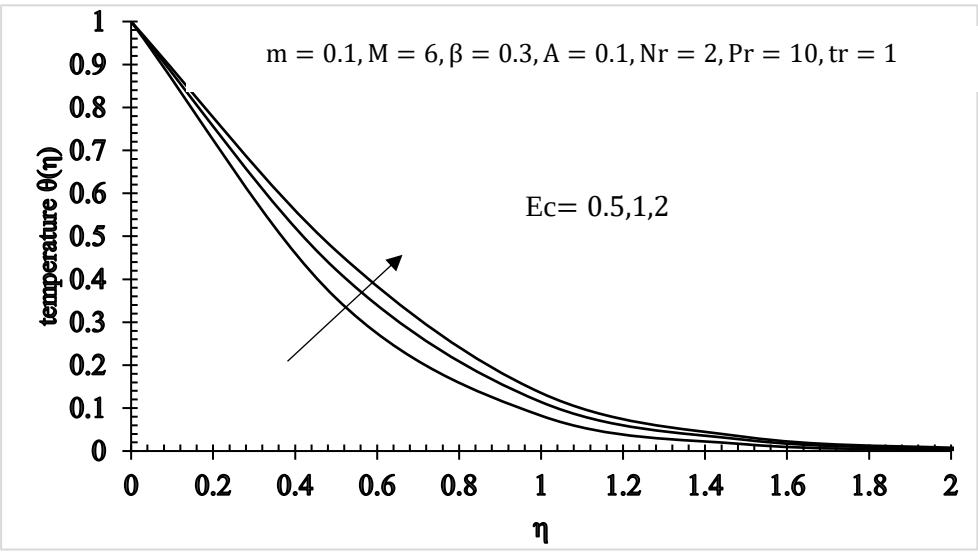

Figure 4.11: Change in $\theta(\eta)$ for ascending values of Ec .

5. Conclusion

Some interesting findings have been listed below.

- Due to the rising values of the magnetic parameter M , the velocity behavior decreases along $x-$ axis in Casson fluid.
- Due to the ascending values of the magnetic parameter M , the temperature behavior also increases in Casson fluid.
- Due to the accelerating values of Hall current m , the velocity rise in $z-$ axis and marginal increment found in χ direction. While the marginal decrement found in the temperature profile in Casson fluid.
- Decrement is observed in the velocity behavior due to the rising values of the unsteadiness A . However, no significant change is prominent in the velocity profile along χ direction in Casson fluid.

▪ An increment is observed in the temperature behavior due to the rising values of the unsteadiness A in Casson fluid.
▪ The fluid flow model presented in the paper has applications in silicon suspensions, blood flow, polymer engineering, and the printing industry.

References

[1] L. J. Crane, "Flow past a stretching plate," *Zeitschrift fur angewandte Mathematik und Physik ZAMP*, vol. 21, no. 4, pp. 645-674, 1970.
[2] E. M. Elbashbeshy, "Heat transfer over a stretching surface with variable surface heat flux," *Journal of Physics D: Applied Physics*, vol. 31, no. 16, pp. 1951, 1998.
[3] T. R. M. a. A. Gupta, "Heat transfer in stagnation-point flow towards a stretching sheet," *Heat and Mass transfer*, vol. 38, no. 6, pp. 517-521, 2002.
[4] R. N. a. I. P. M. Z. Salleh, "Boundary layer flow and heat transfer over a stretching sheet with Newtonian heating," *Journal of the Taiwan Institute of Chemical Engineers*, vol. 41, no. 6, pp. 651-655, 2010.
[5] N. A. a. Z. U. S. M. Misra, "Unsteady boundary layer flow past a stretching plate and heat transfer with variable thermal conductivity," *World Journal of Mechanics*, vol. 2, no. 1, pp. 35, 2012.
[6] K. Pavlov, "Magnetohydrodynamic flow of an incompressible viscous fluid caused by deformation of a plane surface," *Magnitnaya Gidrodinamika*, vol. 4, no. 1, pp. 146-147, 1974.
[7] H. Alfven, "Existence of electromagnetic-hydrodynamic waves," *Nature*, vol. 150, pp. 405, 1942.
[8] T. Sarpkaya, "Flow of non-Newtonian fluids in a magnetic field," Flow of non-Newtonian fluids in a magnetic field", *AIChE Journal*, vol. 7, no. 2, pp. 324-328, 1961.
[9] C. Wang, "Liquid film on an unsteady stretching surface," *Quarterly Journal of Applied Mathematics*, vol. 48, no. 4, pp. 601-610, 1960.
[10] H. Takhar, A. Chamkha and G. Nath, "Unsteady flow and heat transfer on a semi-infinite at plate with an aligned magnetic field," *International Journal of Engineering Science*, vol. 37, no. 13, pp. 1723-1736, 1999.
[11] A. J. Chamkha and A. Al-Mudhaf, "Unsteady heat and mass transfer from a rotating vertical cone with a magnetic field and heat generation or absorption effects," *International journal of thermal sciences*, vol. 44, no. 3, pp. 267-276, 2005.
[12] A. J. Chamkha and S. Ahmed, "Similarity solution for unsteady MHD flow near a stagnation point of a three-dimensional porous body with heat and mass transfer, heat generation/absorption and chemical reaction," *Journal of Applied Fluid Mechanics*, vol. 4, no. 2, pp. 87-94, 2011.
[13] A. Ishak, R. Nazar and I. Pop, "Boundary layer flow and heat transfer over an unsteady stretching vertical surface," *Meccanica*, vol. 44, no. 4, pp. 369-375, 2009.
[14] N. Casson, "A flow equation for pigment-oil suspensions of the printing ink type," *Rheology of Disperse Systems*, pp. 84-104, 1959.
[15] R. Dash, K. Mehta and G. Jayaraman, "Casson fluid flow in a pipe filled with a homogeneous porous medium," *International Journal of Engineering Science*, vol. 34, no. 10, pp. 1145-1156, 1996.
[16] N. Eldabe, G. Saddeck and A. El-Sayed, "Heat transfer of MHD non-Newtonian Casson fluid flow between two rotating cylinders," *Mechanics and Mechanical Engineering* , vol. 5, no. 2, pp. 237-251, 2001.
[17] N. S. Akbar and Z. H. Khan, "Metachronal beating of cilia under the influence of Casson fluid and magnetic field," *Journal of Magnetism and Magnetic Materials*, vol. 378, pp. 320-326, 2015.
[18] N. S. Akbar, "Influence of magnetic field on peristaltic flow of a Casson fluid in an asymmetric channel: application in crude oil refinement," *Journal of Magnetism and Magnetic Materials*, vol. 378, pp. 463-468, 2015.
[19] A. Khalid, I. Khan, A. Khan and S. Shafie Khalid, "Unsteady MHD free convection flow of Casson fluid past over an oscillating vertical plate embedded in a porous medium," *Engineering Science and Technology, an International Journal*, vol. 18, no. 3, pp. 309-317, 2015.
[20] S. A. Shehzad, T. Hayat and A. Alsaedi, "Three-Dimensional MHD Flow of Casson Fluid in Porous Medium with Heat Generation," *Journal of Applied Fluid Mechanics*, vol. 9, no. 1, 2016.

[21] K. Govardhan, G. Narender and G. Sreedhar Sarma, "Viscous dissipation and chemical reaction effects on MHD Casson nanofluid over a stretching sheet," *Malaysian Journal of Fundamental and Applied Sciences*, vol. 15, no. 4, pp. 585-592, 2019.

[22] K. A. Maleque, "MHD Non-Newtonian Casson fluid heat and mass transfer flow with exothermic/endothermic binary chemical reaction and activation energy," *American Journal of Heat and Mass Transfer*, vol. 3, no. 1, pp. 166-185, 2016.

[23] H. Kataria and. H. Patel, "Heat and mass transfer in magnetohydrodynamic (MHD) Casson fluid flow past over an oscillating vertical plate embedded in porous medium with ramped wall temperature," *Propulsion and Power Research*, vol. 7, no. 3, pp. 257-267, 2018.

[24] R. Vijayaragavan and S. Karthikeyan, "Hall Current Effect on Chemically Reacting MHD Casson Fluid Flow with Dufour Effect and Thermal Radiation," *Open Access Quarterly International Journal*, vol. 2, pp. 228-245, 2018.

[25] G. Narender, K. Govardhan and G. Sreedhar Sarma, "Magnetohydrodynamic stagnation point on a Casson nanofluid flow over a radially stretching sheet," *Beilstein J. Nanotechnol*. vol. 11, pp. 1303–1315, 2020

[26] G. Narender, K. Govardhan and G. Sreedhar Sarma, "Viscous dissipation and thermal radiation effects on the flow of Maxwell nanouid over a stretching surface," *Int. J. Nonlinear Anal. Appl.*, vol. 12, no. 2, pp. 1267-1287, 2021.

[27] G. Narender, K. Govardhan and G. Sreedhar Sarma, "MHD Casson Nanofluid Past a Stretching

[28] Sheet with the Effects of Viscous Dissipation, Chemical Reaction and Heat Source/Sink," *J. Appl. Comput. Mech.*, vol. 7, no. 4, pp. 2040–2048, 2021.

[29] Prashu and R. Nandkeolyar, "A numerical treatment of unsteady three-dimensional hydromagnetic flow of a Casson fluid with Hall and radiation effect," *Results in Physics*, vol. 11, pp. 966-974, 2018.